Matter and Radiation at Extremes

Dynamically pre-compressed hydrocarbons studied by self-impedance mismatch

Cite as: Matter Radiat. Extremes 5, 028401 (2020); https://doi.org/10.1063/1.5130726
Submitted: 07 October 2019 . Accepted: 26 December 2019 . Published Online: 27 February 2020

N. J. Hartley, C. Zhang, X. Duan, L. G. Huang, S. Jiang, Y. Li, L. Yang, A. Pelka, Z. Wang, J. Yang, and D. Kraus

COLLECTIONS

This paper was selected as an Editor's Pick

View Online Export Citation CrossMark

ARTICLES YOU MAY BE INTERESTED IN

Understanding the effects of radiative preheat and self-emission from shock heating on equation of state measurement at 100s of Mbar using spherically converging shock waves in a NIF hohlraum
Matter and Radiation at Extremes 5, 018401 (2020); https://doi.org/10.1063/1.5131748

Chemistry under extreme conditions: Pressure evolution of chemical bonding and structure in dense solids
Matter and Radiation at Extremes 5, 018202 (2020); https://doi.org/10.1063/1.5127897

New developments in high-pressure X-ray diffraction beamline for diamond anvil cell at SPring-8
Matter and Radiation at Extremes 5, 018403 (2020); https://doi.org/10.1063/1.5126038

READ NOW!
Matter and Radiation at Extremes
SPECIAL ISSUE: HEDP and ICF Target Fabrication

© 2020 Author(s).

Matter and Radiation at Extremes | RESEARCH ARTICLE | scitation.org/journal/mre

Dynamically pre-compressed hydrocarbons studied by self-impedance mismatch

Cite as: Matter Radiat. Extremes 5, 028401 (2020); doi: 10.1063/1.5130726
Submitted: 7 October 2019 • Accepted: 26 December 2019 •
Published Online: 27 February 2020

View Online Export Citation CrossMark

N. J. Hartley,[1,a] C. Zhang,[2,b] X. Duan,[2] L. G. Huang,[1] S. Jiang,[2] Y. Li,[2] L. Yang,[1,3] A. Pelka,[1,4] Z. Wang,[2] J. Yang,[2] and D. Kraus[1,5]

AFFILIATIONS

[1] Helmholtz-Zentrum Dresden-Rossendorf, 01328 Dresden, Germany
[2] Laser Fusion Research Center, China Academy of Engineering Physics, Mianyang, China
[3] Institute of Fluid Physics, China Academy of Engineering Physics, Mianyang, China
[4] European XFEL GmbH, 22869 Schenefeld, Germany
[5] Technische Universität Dresden, 01062 Dresden, Germany

[a] **Author to whom correspondence should be addressed:** n.hartley@hzdr.de
[b] **Electronic mail:** zhang_lfrc@163.com

ABSTRACT

Using the SG-III prototype laser at China Academy of Engineering Physics, Mianyang, we irradiated polystyrene (CH) samples with a thermal radiation drive, reaching conditions on the principal Hugoniot up to $P \approx 1$ TPa (10 Mbar), and away from the Hugoniot up to $P \approx 300$ GPa (3 Mbar). The response of each sample was measured with a velocity interferometry diagnostic to determine the material and shock velocity, and hence the conditions reached, and the reflectivity of the sample, from which changes in the conductivity can be inferred. By applying the self-impedance mismatch technique with the measured velocities, the pressure and density of thermodynamic points away from the principal Hugoniot were determined. Our results show an unexpectedly large reflectivity at the highest shock pressures, while the off-Hugoniot points agree with previous work suggesting that shock-compressed CH conductivity is primarily temperature-dependent.

© 2020 Author(s). All article content, except where otherwise noted, is licensed under a Creative Commons Attribution (CC BY) license (http://creativecommons.org/licenses/by/4.0/). https://doi.org/10.1063/1.5130726

I. INTRODUCTION

The behavior of hydrocarbons under extreme conditions is of great interest across the field of high-energy-density science. Consisting of two of the most common elements within giant planets, they serve as an excellent example for study of the behavior of planetary interiors.[1,2] In addition, they are used as pushers for shock compression experiments on other materials[3] and to contain deuterium–tritium mixtures in inertial confinement fusion experiments.[4] Although in many of these cases, the material is driven by a single shock, and so the state reached can be described by the Rankine–Hugoniot relations, the conditions in so-called off-Hugoniot states—reached by either ramp compression or subsequent shocks—are also important, but are significantly harder to determine.

In an experiment, off-Hugoniot states will tend to have a lower temperature than if the same pressure were reached with single shock. This is easily shown for a polytropic gas, where the entropy increases as a function of the pressure ratio P_1/P_0 across the shock such that multiple weaker compressions give a smaller rise in entropy,[5,6] and this becomes an increasingly good approximation for shock-compressed material with increasing pressure. When considering compression by multiple shocks, the limiting case is ramp compression, which is ideally isentropic.[7,8] In the case of low-impedance materials such as plastic, however, the requirements on the shape of the driving pulse are very strict to avoid unintentionally driving shocks into the sample.[9] Consequently, multiple subsequent shocks offer a more forgiving way to reach lower-temperature conditions, with more room for variation in the driving pulse shape.

The principal difficulty in studying off-Hugoniot states experimentally is the lack of previous experimental data. While there exists (e.g., in the case of plastics) a large body of work from single-shock compressed samples,[10–12] the lack of benchmarking data away from the Hugoniot means that simulations of these states, which are commonly used to estimate the conditions, will necessarily have a significantly larger uncertainty. Impedance mismatch is a technique commonly used to determine the thermodynamic state of a material undergoing a single shock, by comparing it with the response of a

material with a well-known shock Hugoniot.[5] Recent work by Guarguaglini *et al.*[13] described the application of a similar technique to determine the behavior of a water sample undergoing multiple compressions, which we apply here to polystyrene samples.

This paper presents measured results for the pressure, density, and reflectivity of polystyrene $(C_8H_8)_n$, referred to here as CH. The samples were compressed by single and double shocks, and the results are compared with data previously taken at the OMEGA laser facility.[11] At pressures reached by a single shock, we observe higher than expected reflectivity; under double-shocked conditions, the reflectivity is lower than would be expected for the same pressure in a single shock, but shows a similar relationship as a function of simulated temperature. This may indicate that the metallization of CH at the shock front is primarily temperature-dependent.

II. EXPERIMENT

The experiment was carried out using the Shenguang-III prototype laser, located at the Research Center of Laser Fusion (LFRC) at the China Academy of Engineering Physics (CAEP) in Mianyang, China.[14,15] It is a frequency-tripled (wavelength λ = 355 nm) laser facility consisting of eight beams, each with a maximum output of 800 J, and a maximum instantaneous power (for shaped pulses) of 1 TW; the pulse shapes here used up to 800 J in 2 ns for the square pulse, and 225 J total in 4 ns for the step pulse. They are focused to a spot of diameter 500 μm and smoothed with continuous phase plates. The pulses can be shaped arbitrarily within a window of 10 ns. As illustrated in Fig. 1, the lasers deliver the energy onto a gold hohlraum, generating a high-energy thermal X-ray spectrum, which deposits energy into the target package. The target in this experiment consisted of an aluminum ablator layer to absorb the energy and drive the shock, a gold layer to reduce radiation preheating, and a further aluminum layer to minimize impedance mismatch with the plastic sample itself. This Al–Au–Al package was glued onto the plastic sample, with pressure applied to minimize the thickness of the glue layer. This indirect drive method should allow a much smoother shock front than would be driven by direct irradiation from a high-energy laser.[16]

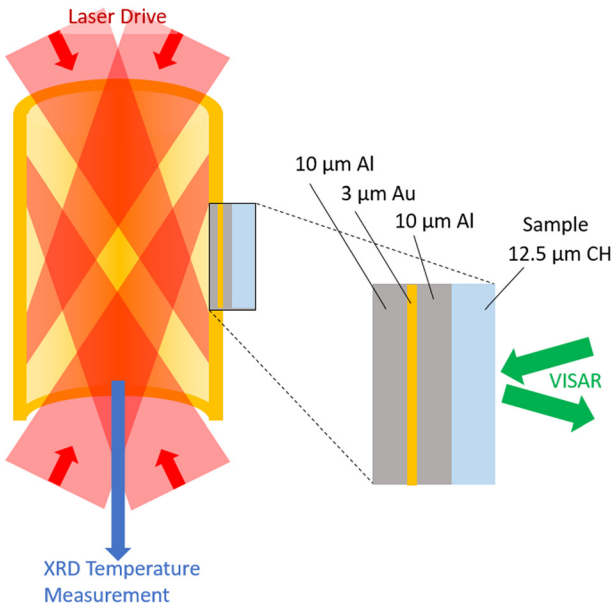

FIG. 1. Cartoon of the experimental setup, showing the hohlraum and the target package, consisting of Al–Au–Al layers attached to the CH sample. The driving radiation temperature is monitored on the XRD cameras, and shock propagation data are taken on the VISAR system.

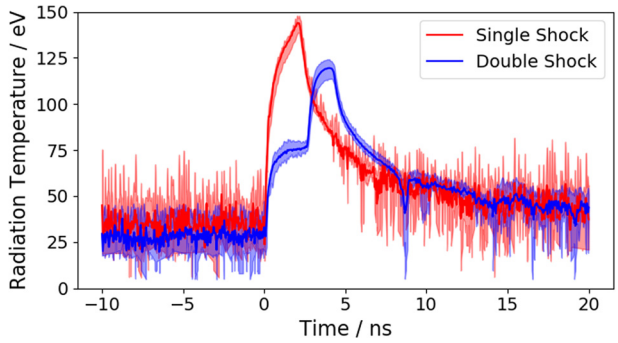

FIG. 2. Examples of the measured radiation temperature incident on the ablator surface as a function of time for the cases of a single and a double shock. The shaded uncertainty is the variation in measured temperature between the cameras. The lineouts correspond to the temperatures in shots 302 and 315, respectively (see Table I in the Appendix).

The soft X-ray spectrum generated in the hohlraum was monitored by X-ray diode (XRD) detectors; examples of the temporal evolution of the temperature for the single- and double-shock cases are shown in Fig. 2, with the shaded area indicating the range of temperatures from the different cameras. The conditions reached in the sample due to this incoming radiation can be estimated using radiation hydrodynamics simulation. For this work, we used the HELIOS code,[17] together with SESAME equations of state (EOS) 3719, 2700, and 5792 for the aluminum, gold, and polystyrene,

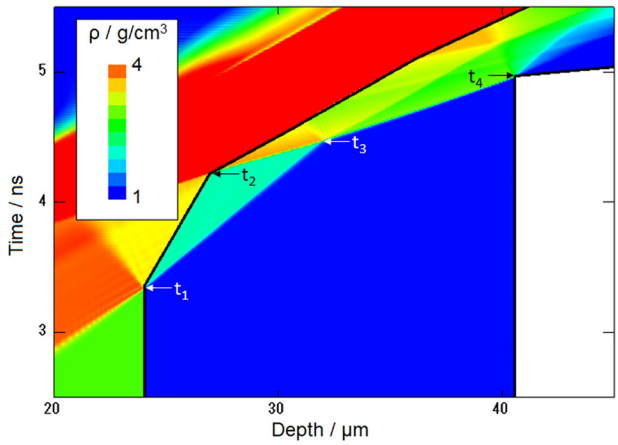

FIG. 3. Plastic target density, simulated using the double-shock radiation profile in the radiation hydrodynamics code HELIOS, with SESAME equation of state 7592 for polystyrene. The radiation is incident from the left-hand edge onto the ablator; the shock passes through this and into the CH, the boundaries of which are marked by the black lines. The coordinates are Eulerian, allowing the different shock-front velocities to be observed.

©Author(s) 2020

respectively,[18] and PROPACEOS opacities;[19] for the gold layer, the opacity of copper was used, with the differences in opacity at the relevant radiation temperatures being expected to be negligible. The result of the simulation using the double-shock temperature profile is shown in Fig. 3, with the two shocks entering the plastic sample at t_1 and t_2, merging to form a single strong shock at t_3, and breaking out of the rear surface at t_4; the double-shocked off-Hugoniot regions are therefore only present for the short time between t_2 and t_3.

The behavior of the sample was monitored using two velocity interferometer system for any reflector (VISAR) arms, at a probe wavelength of 532 nm. The velocity per fringe (VPF) parameters of the left and right arms were 7.116 km/s and 4.981 km/s, respectively. The time windows for the VISAR data acquisition were generally around 10 ns (9.76 ns on the left arm and 10.27 ns on the right arm), although some shots used a 5.45 ns time window on the right arm to give finer time resolution.

III. ANALYSIS

A. Self-impedance mismatch technique

The self-impedance mismatch technique determines the state of a double-shocked material from the initial and final conditions, both of which lie on the Hugoniot, and the speed of the second shock. A full description of the method can be found in the paper by Guarguaglini *et al.*,[13] a condensed version of which follows here.

Considering the example shown in Fig. 4, the single-shocked state P1 is first measured, in this case by determining the particle speed $u_{p,1}$ observed through the transparent first shock. By conservation of momentum across the second shock, the state P2 reached after the shock must lie along a Rayleigh line from these initial conditions, described by

$$P(u_p) = P_1 + \rho_1 (u_{s,2} - u_{p,1})(u_p - u_{p,1}), \tag{1}$$

with $u_{s,2}$ the velocity of the second shock. The conditions after the final (merged) shock, at P3, are found from the VISAR fringe shift of the merged shock, which travels with velocity $u_{s,m}$, thus defining a point on the Hugoniot. This final point must also lie on the adiabatic release path from point P2, which is approximated by the mirror reflection of the principal Hugoniot around the line $u_p = u_{p,m}$. Since the relevant portion of this line is short, this approximation is not a significant source of error. The pressure and material velocity of the double-shocked state P2 are then determined from the intersection of the Rayleigh and release lines, and the density from mass conservation:

$$\rho_2 = \rho_1 \frac{u_{s,2} - u_{p,1}}{u_{s,2} - u_{p,2}}. \tag{2}$$

B. Application and results

An example of the VISAR data is shown in Fig. 5, along with the inferred velocities. We first consider the behavior after the initial shock enters the sample at t_1. At the pressures reached here, polystyrene remains transparent, and so the VISAR signal observed is reflected from the (now moving) Al–CH interface. This interface moves with particle velocity $u_{p,1}$, behind the shock traveling at velocity $u_{s,1}$. The VISAR system measures an apparent velocity u_{app}, related to the fringe shift $F(t)$ by

$$\begin{aligned} u_{\mathrm{app}}(t) &= \mathrm{VPF} \times F(t) \\ &= n_1 u_{p,1} - (n_1 - n_0) u_{s,1}, \end{aligned} \tag{3}$$

with VPF the velocity-per-fringe parameter of the VISAR setup, and n_0 and n_1 the indices of refraction of the sample material before and after the shock.

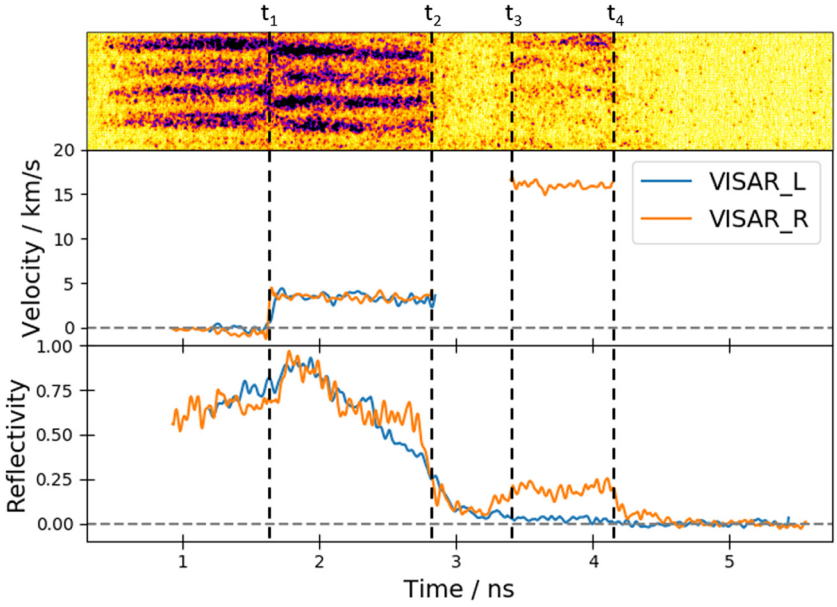

FIG. 4. VISAR data, calculated velocities, and corresponding reflectivity values. Between t_1 and t_2, the value is equal to the apparent particle velocity u_{app}, while the higher velocity from t_3 to t_4, seen only on one of the VISAR arms, is due to the merged shock $u_{s,m}$. The reflectivity values show a rise after the first shock enters the plastic, possibly due to changes in the Al–CH interface, with the horizontal dashed line showing the theoretical Al–plastic reflectivity of 88%. The flat region of nonzero reflectivity between t_2 and t_3 provides the reflectivity value for the double-shocked state. The data are from shot 315 (see Table I in the Appendix).

©Author(s) 2020

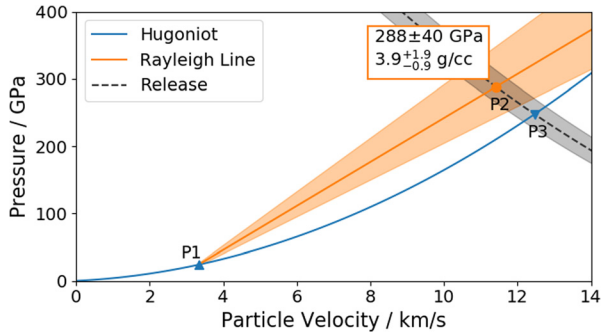

FIG. 5. Example of the self-impedance mismatch technique illustrated on the P-u_p plane. The double-shocked state P2 is determined by the intersection of the Rayleigh line from the single-shocked state P1 and the release line of the final state P3. The uncertainty in the Rayleigh line, indicated by the shaded orange area, is due to the uncertainty in the transit time, and hence the shock speed $u_{s,2}$, while the shaded gray area is due to uncertainty in the merged shock velocity $u_{s,m}$, and hence the final state. The uncertainties in pressure and density are taken from the intersection of the shaded areas, and are particularly large for the density ρ.

In the case of polystyrene, the change in the index of refraction after shock compression has been well studied; using the empirical relations for $n(P)$ from Zhang *et al.*[12] and combining them with known u_s–u_p relations,[10] we find that, for pressures above 20 GPa, they are related by

$$u_{\mathrm{app}} = (1.25 \times u_{p,1}) - 0.58, \tag{4}$$

with the velocities in units of km/s. For the example presented in Fig. 4 (shot 313 in Table I in the Appendix), we find an apparent velocity $u_{\mathrm{app}} = 3.13 \pm 0.10$ km/s for a particle velocity $u_{p,1} = 3.33 \pm 0.10$ km/s, corresponding to a pressure $P_1 = 24.5 \pm 1.5$ GPa.

For the final state reached by the single merged shock, after time t_3, the VISAR laser reflects from the shock front, and so the apparent velocity is related to the shock velocity by

$$u_{\mathrm{app}} = n_0 u_s. \tag{5}$$

We thus obtain the merged shock speed $u_{s,m}$ from the measured velocity. For the example, we find $u_{s,m} = 18.9 \pm 0.3$ km/s, corresponding to a pressure $P_3 = 249 \pm 11$ GPa. In the case of a single strong shock, this is the only step: for the relevant shots, we measured shock speeds $u_s = 21.5 \pm 0.2$ km/s and $u_s = 31.7 \pm 0.5$ km/s, equivalent to pressures $P = 362 \pm 23$ GPa and $P = 963 \pm 97$ GPa.

The last quantity to be extracted from the VISAR data is the speed of the second shock $u_{s,2}$, which is necessary to define the slope of the Rayleigh line. Under the conditions reached in this experiment, this shock is only very weakly reflecting, and so the velocity cannot be calculated from fringe shifts, but must instead be deduced from transit time measurements and the initial shock and particle speeds. In the case considered, we find a transit time $\Delta t = t_3 - t_2 = 0.25 \pm 0.04$ ns, for a shock velocity $u_{s,2} = 19.8^{+3.7}_{-2.7}$ km/s.

Substituting the measured velocities into Eqs. (1) and (2), we find the conditions of the double-shocked state to be $P = 288 \pm 40$ GPa and $\rho = 3.9^{+1.9}_{-0.9}$ g/cm^3, with the asymmetric error in the density being due to the uncertainty in the second shock velocity $u_{s,2}$. The uncertainties are estimated from the limits of the overlapping shaded area, with the density extremes coming from the points closest to and furthest from the Hugoniot line. A second shot, with a slightly lower temperature drive, drove the sample to double-shocked conditions $P = 199 \pm 30$ GPa and $\rho = 3.6^{+1.4}_{-0.6}$ g/cm^3.

While this does demonstrate the capability of the self-impedance mismatch technique to directly determine off-Hugoniot conditions, the results, particularly for the density, show very large error bars. Since this is due mainly to the uncertainty in the second shock speed $u_{s,2}$, future experiments could consider approaches to determine this more precisely. While the best way to do this would be driving a shock that was strong enough to be reflecting, so that it could be measured directly, the interface with the pre-compressed material means that it would probably need to be so strong that the benefits of the double-shock drive would be lost, since we would be beyond conditions relevant for planetary interiors. Instead, a thicker plastic sample, and a longer delay between the shocks entering it, should increase the time $t_2 - t_3$, such that an uncertainty of the order of ±0.04 ns has a smaller overall effect.

Although we were not able to measure the temperatures directly in this experiment, we have estimated them from known equation-of-state (EOS) data, using SESAME equation of state 7592 for polystyrene. The temperatures were estimated from the measured (P, ρ) position, with the uncertainty in the temperature arising solely from uncertainties in these quantities. This is slightly less than would be expected if the temperature were measured directly, such as by streaked optical pyrometry,[11] and reflects systematic uncertainties in temperature EOS data. Away from the Hugoniot, the results are again more complicated, and the EOS data are less well benchmarked. Using the (P, ρ) values measured and their associated uncertainties results in highly unphysical values: for instance, shot 315, presented in Fig. 5, gives $T = -0.55^{+1.83}_{-5.23}$ eV. Rather than using these values, and to meaningfully compare our results with tabulated EOS values, we have performed radiation hydrodynamics simulations, tuning the input intensity to reproduce the measured pressure and shock transit and coalescence times. These give lower densities than our method, although easily within the error bars: specifically, $\rho = 3.35$ g/cm^3 for shot 313 at $P = 288 \pm 40$ GPa and $\rho = 3.27$ g/cm^3 for shot 315, with $P = 199 \pm 30$ GPa. Our estimates of the temperature then use these pressures and densities, with the uncertainty in the pressure again leading to the uncertainty in the temperature—these uncertainties are much larger than those at similar pressures on the Hugoniot, owing to the lack of benchmarking. The results are shown in Fig. 6 and suggest that the drive is capable of reaching conditions relevant to the diamond formation previously observed,[1] but also that the temperature estimate for the double-shocked point at ~300 GPa is likely incorrect, since it is significantly above the secondary Hugoniot starting at 30 GPa.

C. Reflectivity

As well as the fringe shift, the VISAR data can be used to extract values for the reflectivity of the sample, in both the single- and double-shocked states. The reflectivity values are calculated by first subtracting the average value at late times ($t > 3.5$ ns for the example in Fig. 7), to account for background signal on the detector, which is assumed to be constant in time. The lineout is then multiplied by the reflectivity of Al, to give the absolute reflectivity of the shock–ambient interface. The reflectivity of Al in contact with CH is assumed to take the ideal Fresnel value of 88%, since we did not measure the absolute reflectivity of each target before the shot. The quoted reflectivity values also account for reflection from the rear CH–vacuum interface, which is of the order of 5%; for the large reflectivity values from the

© Author(s) 2020

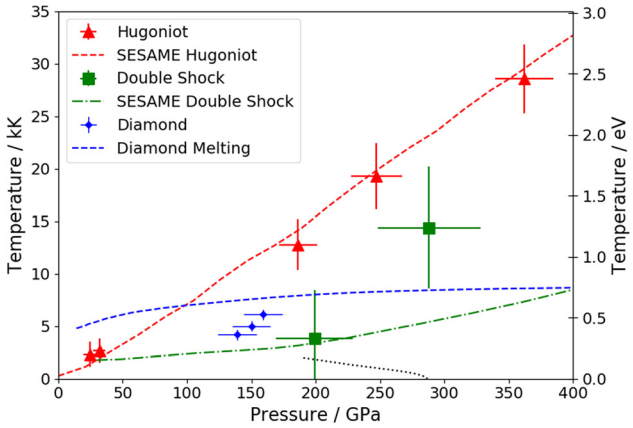

FIG. 6. Pressure–temperature phase diagram, showing the conditions reached on the Hugoniot (red triangles and dashed line), and with the double-shock drive (green squares and dot-dashed line); the highest-pressure point on the Hugoniot is omitted so that the lower-temperature results can be distinguished. Also shown are the conditions where diamond formation from double-shocked CH was observed by Kraus *et al.*[1] (blue diamonds), the expected melting line of diamond from Wang *et al.*[20] (blue dashed line), and the hydrocarbon demixing boundary from Gao *et al.*[21] (black dotted line).

single-shock states, this is a negligible effect, but is a significant fraction of the observed signal for the weakly reflecting cases.

These measured reflectivity values can be compared with previous data from highly compressed hydrocarbon samples, taken by Barrios *et al.*[11] at the same probing wavelength $\lambda = 532$ nm, and from the quantum molecular dynamics (QMD) simulations of Hu *et al.*,[22] using either the HSE or PBE exchange correlation functional. As expected, the reflectivity increases rapidly along the Hugoniot. At the highest pressures reached by single shocks, however, we observe significantly higher reflectivity than the limit seen in QMD and previous results.[11,23] This is not due to an error in the choice of interface material, as was the case in previous experimental comparisons.[24,25] Figure 7 shows an example reflectivity lineout from the shot that reached 362 GPa, which appears to clearly show a reflectivity above the expected high-pressure limit of $R \sim 0.4$ in both VISAR arms. However, the reflectivities from lower-pressure shots, such as that seen in Fig. 5, show an increase as the first shock passes this interface. On these shots, this maximum value is used for normalization, but for high-pressure shots, where the shock in the plastic is reflecting, this is not possible. This does, however, indicate a systematic uncertainty due to the normalization, which we have not attempted to account for, and underlines the significance of properly calibrating the targets.

While the normalization issue is less of an issue for the double-shock shots, comparing the reflectivity results with previous work is more challenging. Since they are not expected to be transparent, the refractive index n_2 must be replaced with its complex value $\mathbf{n}_2 = n_2 + i\kappa$. The reflectivity is therefore equal to

$$R = \left|\frac{n_2 + i\kappa - n_1}{n_2 + i\kappa + n_1}\right|^2 \tag{6}$$

$$= 1 - \frac{4n_2 n_1}{(n_2 + n_1)^2 + \kappa^2}, \tag{7}$$

with Eq. (7) being valid if n_2, n_1, and κ are all positive. The value n_1 is equal to the refractive index in the pre-compressed CH, since the reflection is from the second shock front, and can be estimated from the pressure-dependent refractive index $n(P)$ of Zhang *et al.*[12]

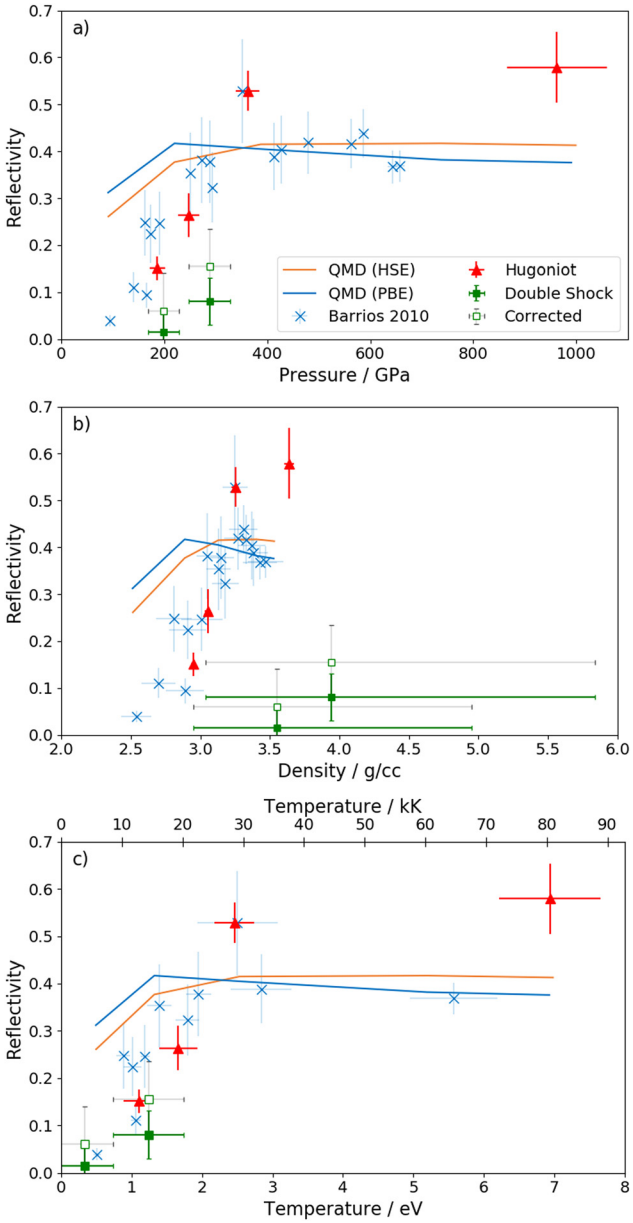

FIG. 7. Reflectivity of shocked polystyrene as a function of (a) pressure, (b) density, and (c) temperature, all taken with probing wavelength $\lambda = 532$ nm. The red triangles show points on the Hugoniot, either from single shocks or from the final-state merged shocks, while the green squares show double-shocked conditions. The closed and open green squares show reflectivity values before and after correction, respectively, as described in the text. The blue crosses are results from the OMEGA facility, taken from Barrios *et al.*[11] The disagreement at high pressures is likely due to a systematic offset in the initial reflectivity, as this was not measured prior to the shot.

© Author(s) 2020

However, this still does not allow both components of $\mathbf{n}_2$ to be determined from a single measurement of the reflectivity.

To compare the double-shocked states with states on the Hugoniot, we would like to "correct" the measured reflectivity to give the value that would be expected if it were adjacent to the uncompressed, rather than pre-compressed, CH, i.e., evaluating Eq. (6) with n_0 instead of n_1. We first assume that the double-shocked state can be represented by a purely real refractive index $n_{2,r}$, which can be calculated from Eq. (6) with $\kappa = 0$ and the relevant $n_1 = n(P_1)$. This value $n_{2,r}$ is the maximum value of the real part of $\mathbf{n}_2 = n_2 + i\kappa$, as can be seen from Eq. (7). For any lower value $n_2 < n_{2,r}$, a value of κ can be chosen such that it matches the observed reflectivity.

The value $n_{2,r}$ can be used along with the ambient CH n_0 to give a "corrected" reflectivity from the double-shocked state. Alternatively, any of the (n_2, κ) pairs that reproduced the observed reflectivity can be used. It is empirically seen that the maximum corrected value for the reflectivity is that calculated with $n_2 = n_{2,r}$ and $\kappa = 0$. Therefore, the corrected reflectivity that can be obtained under this simplifying assumption is the maximum possible value that the reflectivity could take, and accounting for the extinction coefficient in the refractive index, κ, would reduce the corrected value. These maximum corrected values are plotted in Fig. 8, where they are already observed to be noticeably below those of the single-shocked states, with the disparity as a function of density being particularly large, notwithstanding the significant error bars.

The estimated temperatures are used for the plot in Fig. 8(c), where we see that the reflectivities from the off-Hugoniot states are generally consistent with the reflectivity as a function of temperature for the on-Hugoniot states, unlike for density or pressure, although a more direct measurement of the temperature would be useful to confirm this relationship. Nevertheless, this is strong evidence that, as suggested in the work of Zhang *et al.*,[12] temperature is the primary cause of the conductivity increase in polystyrene, as is the case in water.[26] The sharp rise and saturation in the reflectivity is characteristic of an insulator–conductor transition, as is seen in, for example, deuterium,[27] diamond,[28] and liquid mixtures.[29] This may suggest that, even away from the Hugoniot, CH undergoes the same metallization process, and that it does not appear to be influenced by the formation of diamond that has previously been seen under similar conditions.[1] On the other hand, the measurements here are restricted to the shock front, unlike X-ray diffraction techniques, which are able to probe the full thickness of the target. This may indicate that the formation of diamond from shock-compressed CH, and any possible effects of this on the conductivity of the sample, occur over longer time scales and so cannot be captured by an optical probing diagnostic. Further work would therefore be required to determine the evolution of the conductivity after the shock transit.

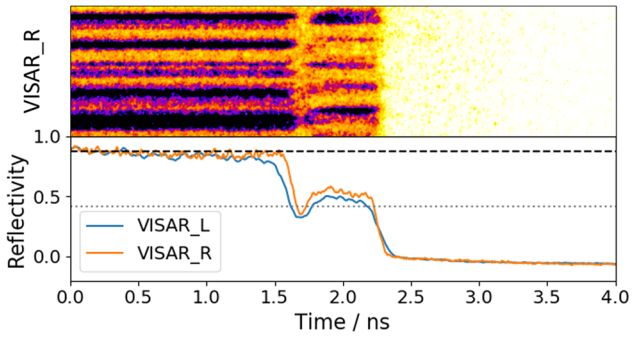

FIG. 8. Example showing reflectivity for the single-shock shot at 362 GPa (shot 302 in Table I in the Appendix), as measured on each arm of the VISAR system, and assuming that the initial reflectivity is equal to the theoretical reflectivity of Al, equal to 88% (black dashed line). The reflectivity in the shocked region is equal to 53% ± 3%, with the uncertainty being due to the different values from each arm and to uncertainty in the fitting to the initial Al value. The gray dotted line indicates the maximum reflectivity expected from the QMD theoretical results.

IV. CONCLUSION

We have demonstrated that self-impedance mismatch has the capability to apply the results of Hugoniot measurements on plastics to directly determine conditions away from the principal Hugoniot. Such conditions are important for studying the behavior of materials under a much wider range of conditions, with particular relevance for planetary interiors, since single-shock compression to planetary-relevant pressures reaches far higher temperatures than are believed to exist within such bodies. At high shock pressures, our results seem to indicate a higher than expected reflectivity, and further work would be required to confirm this. At conditions away from the Hugoniot, the observed shock-front reflectivity is below that expected for Hugoniot points at the same pressure or density, but, using temperatures estimated from simulations, the reflectivities agree better. This may indicate that the metallization behavior is the same at both on- and off-Hugoniot states, with implications for planetary interiors, or may not hold true as the carbon demixes and forms diamond at later times. Future work with direct temperature measurement, such as by streaked optical pyrometry, would provide greater certainty about the EOS behavior under such double-shocked conditions and would serve as a benchmark for simulation codes.

ACKNOWLEDGMENTS

The authors would like to thank the technical teams at LFRC for their invaluable work producing the targets and operating the facility. N.J.H. and D.K. were supported by the Helmholtz Association under Grant No. VH-NG-1141. Y.L. was supported by the National Natural Science Foundation of China (Grant No. 11605189).

APPENDIX: RESULTS TABLE

TABLE I. Data presented in the plots in Fig. 8.

Shot[a]	P (GPa)	ρ (g/cm^3)	R[b]	T (eV)[c]
301	963 ± 97	3.63 ± 0.04	*0.58 ± 0.07*	6.94 ± 0.72
302	362 ± 23	3.25 ± 0.03	*0.53 ± 0.04*	2.46 ± 0.28
313	249 ± 11	3.05 ± 0.02	0.26 ± 0.05	1.66 ± 0.27
315	186 ± 10	2.95 ± 0.02	0.15 ± 0.03	1.10 ± 0.21
313d	288 ± 43	$3.94^{+1.9}_{-0.9}$	0.16 ± 0.08	1.24 ± 0.50
315d	199 ± 33	$3.55^{+1.4}_{-0.6}$	0.06 ± 0.08	0.33 ± 0.40

[a]The shots marked with "d" are conditions in the double-shocked region.
[b]Reflectivity values at wavelength $\lambda = 532$ nm, with results in italics those with possible systematic uncertainty from the normalization.
[c]1 eV = 11 605 K.

©Author(s) 2020

REFERENCES

[1]D. Kraus, J. Vorberger, A. Pak, N. J. Hartley, L. B. Fletcher, S. Frydrych, E. Galtier, E. J. Gamboa, D. O. Gericke, S. H. Glenzer, E. Granados, M. J. MacDonald, A. J. MacKinnon, E. E. McBride, I. Nam, P. Neumayer, M. Roth, A. M. Saunders, A. K. Schuster, P. Sun, T. van Driel, T. Döppner, and R. W. Falcone, "Formation of diamonds in laser-compressed hydrocarbons at planetary interior conditions," Nat. Astron. **1**, 606–611 (2017).

[2]D. Kraus, N. J. Hartley, S. Frydrych, A. K. Schuster, K. Rohatsch, M. Rödel, T. E. Cowan, S. Brown, E. Cunningham, T. van Driel, L. B. Fletcher, E. Galtier, E. J. Gamboa, A. Laso Garcia, D. O. Gericke, E. Granados, P. A. Heimann, H. J. Lee, M. J. MacDonald, A. J. MacKinnon, E. E. McBride, I. Nam, P. Neumayer, A. Pak, A. Pelka, I. Prencipe, A. Ravasio, R. Redmer, A. M. Saunders, M. Schölmerich, M. Schörner, P. Sun, S. J. Turner, A. Zettl, R. W. Falcone, S. H. Glenzer, T. Döppner, and J. Vorberger, "High-pressure chemistry of hydrocarbons relevant to planetary interiors and inertial confinement fusion," Phys. Plasmas **25**, 056313 (2018).

[3]I. Prencipe, J. Fuchs, S. Pascarelli, D. Schumacher, R. Stephens, N. B. Alexander, R. Briggs, M. Büscher, M. Cernaianu, A. Choukourov, M. De Marco, A. Erbe, J. Fassbender, G. Fiquet, P. Fitzsimmons, C. Gheorghiu, J. Hund, L. Huang, M. Harmand, N. J. Hartley, A. Irman, T. Kluge, Z. Konopkova, S. Kraft, D. Kraus, V. Leca, D. Margarone, J. Metzkes, K. Nagai, W. Nazarov, P. Lutoslawski, D. Papp, M. Passoni, A. Pelka, J. Perin, J. Schulz, M. Smid, C. Spindloe, S. Steinke, R. Torchio, C. Vass, T. Wiste, R. Zaffino, K. Zeil, T. Tschentscher, U. Schramm, and T. Cowan, "Targets for high repetition rate laser facilities: Needs, challenges and perspectives," High Power Laser Sci. Eng. **5**, e17 (2017).

[4]A. Kritcher, D. Clark, S. Haan, S. Yi, A. Kritcher, S. Haan, S. Yi, A. Zylstra, J. Ralph, and C. Weber, "Comparison of the three NIF ablators," Technical Report No. LLNL-TR-739464, Lawrence Livermore National Laboratory (LLNL), Livermore, CA, 2017.

[5]R. P. Drake, *High-Energy-Density Physics* (Springer-Verlag, Berlin, 2006).

[6]P. McKenna, D. Neely, R. Bingham, and D. Aroszynski, *Laser-Plasma Interactions and Applications* (Springer, 2013).

[7]R. F. Smith, J. H. Eggert, A. Jankowski, P. M. Celliers, M. J. Edwards, Y. M. Gupta, J. R. Asay, and G. Collins, "Stiff response of aluminum under ultrafast shockless compression to 110 GPA," Phys. Rev. Lett. **98**, 065701 (2007).

[8]M. D. Knudson, M. P. Desjarlais, A. Becker, R. W. Lemke, K. R. Cochrane, M. E. Savage, D. E. Bliss, T. R. Mattson, and R. Redmer, "Direct observation of an abrupt insulator-to-metal transition in dense liquid deuterium," Science **348**, 1455–1460 (2015).

[9]D. C. Swift and R. G. Kraus, "Properties of plastic ablators in laser-driven material dynamics experiments," Phys. Rev. E **77**, 066402 (2008).

[10]S. P. Marsh, LASL Shock Hugoniot Data, 1980.

[11]M. A. Barrios, D. G. Hicks, T. R. Boehly, D. E. Fratanduono, J. H. Eggert, P. M. Celliers, G. W. Collins, and D. D. Meyerhofer, "High-precision measurements of the equation of state of hydrocarbons at 1–10 Mbar using laser-driven shock waves," Phys. Plasmas **17**, 056307 (2010).

[12]X. Zhang, G. Wang, B. Luo, F. Tan, S. N. Bland, J. Zhao, C. Sun, and C. Liu, "Refractive index and polarizability of polystyrene under shock compression," J. Mater. Sci. **53**(17), 12628–12640 (2018).

[13]M. Guarguaglini, J. A. Hernandez, A. Benuzzi-Mounaix, R. Bolis, E. Brambrink, T. Vinci, and A. Ravasio, "Characterising equation of state and optical properties of dynamically pre-compressed materials," Phys. Plasmas **26**, 042704 (2019).

[14]W. Zheng, X. Wei, Q. Zhu, F. Jing, D. Hu, J. Su, K. Zheng, X. Yuan, H. Zhou, W. Dai, W. Zhou, F. Wang, D. Xu, X. Xie, B. Feng, Z. Peng, L. Guo, Y. Chen, X. Zhang, L. Liu, D. Lin, Z. Dang, Y. Xiang, and X. Deng, "Laser performance of the SG-III laser facility," High Power Laser Sci. Eng. **4**, e21 (2016).

[15]T. Gong, L. Hao, Z. Li, D. Yang, S. Li, X. Li, L. Guo, S. Zou, Y. Liu, X. Jiang, X. Peng, T. Xu, X. Liu, Y. Li, C. Zheng, H. Cai, Z. Liu, J. Zheng, Z. Wang, Q. Li, P. Li, R. Zhang, Y. Zhang, F. Wang, D. Wang, F. Wang, S. Liu, J. Yang, S. Jiang, B. Zhang, and Y. Ding, "Recent research progress of laser plasma interactions in Shenguang laser facilities," Matter Radiat. Extremes **4**, 055202 (2019).

[16]Z. Zhang, Y. Zhao, J. Zhang, Z. Hu, L. Jing, B. Qing, G. Xiong, M. Lv, H. Du, Y. Yang, X. Zhan, R. Yu, Y. Mei, and J. Yang, "Radiation flux study of hohlraum used to create uniform and strongly coupled warm dense matter," Phys. Plasmas **26**, 072704 (2019).

[17]J. J. MacFarlane, I. E. Golovkin, and P. R. Woodruff, "HELIOS-CR—A 1-D radiation-magnetohydrodynamics code with inline atomic kinetics modeling," J. Quant. Spectrosc. Radiat. Transfer **99**, 381–397 (2006).

[18]S. P. Lyon and J. D. Johnson, "SESAME: Los Alamos National Laboratory equation of state database 1992," Technical Report No. LA-UR-92-3047, LANL, Los Alamos, 1992.

[19]J. J. MacFarlane, I. E. Golovkin, P. R. Woodruff, D. R. Welch, B. V. Oliver, T. A. Mehlhorn, and R. B. Campbell, "Simulation of the ionization dynamics of aluminum irradiated by intense short-pulse lasers," in *Inertial Fusion Sciences and Applications 2003*, edited by B. A. Hammel, D. D. Meyerhofer, and J. Meyer-ter-Vehn (American Nuclear Society, 2004), p. 457.

[20]Z. Wang, J. Zheng, B. Zhao, C. X. Yu, X. Jiang, W. Li, S. Liu, Y. Ding, and Z. Zheng, "Thomson scattering from laser-produced gold plasmas in radiation conversion layer," Phys. Plasmas **12**, 082703 (2005).

[21]G. Gao, A. R. Oganov, Y. Ma, H. Wang, P. Li, Y. Li, T. Iitaka, and G. Zou, "Dissociation of methane under high pressure," J. Chem. Phys. **133**, 144508 (2010).

[22]S. X. Hu, L. A. Collins, T. R. Boehly, Y. H. Ding, P. B. Radha, V. N. Goncharov, V. V. Karasiev, G. W. Collins, S. P. Regan, and E. M. Campbell, "A review on *ab initio* studies of static, transport, and optical properties of polystyrene under extreme conditions for inertial confinement fusion applications," Phys. Plasmas **25**, 056306 (2018).

[23]N. Ozaki, T. Sano, M. Ikoma, K. Shigemori, T. Kimura, K. Miyanishi, T. Vinci, F. H. Ree, H. Azechi, T. Endo, Y. Hironaka, Y. Hori, A. Iwamoto, T. Kadono, H. Nagatomo, M. Nakai, T. Norimatsu, T. Okuchi, K. Otani, T. Sakaiya, K. Shimizu, A. Shiroshita, A. Sunahara, H. Takahashi, and R. Kodama, "Shock hugoniot and temperature data for polystyrene obtained with quartz standard," Phys. Plasmas **16**, 062702 (2009).

[24]M. Koenig, F. Philippe, A. Benuzzi-Mounaix, D. Batani, M. Tomasini, E. Henry, and T. Hall, "Optical properties of highly compressed polystyrene using laser-driven shockwaves," Phys. Plasmas **10**, 3026–3029 (2003).

[25]S. X. Hu, T. R. Boehly, and L. A. Collins, "Properties of warm dense polystyrene plasmas along the principal Hugoniot," Phys. Rev. E **89**, 063104 (2014).

[26]J. Li, H. Shu, Y. Sun, H. Zhang, J. Yang, Q. Wu, and J. Hu, "Electronic bandgap of water in the superionic and plasma phases," Phys. Plasmas **26**, 092703 (2019).

[27]P. M. Celliers, M. Millot, S. Brygoo, R. S. Mcwilliams, D. E. Fratanduono, J. R. Rygg, A. F. Goncharov, P. Loubeyre, J. H. Eggert, J. L. Peterson, N. Meezan, S. Le Pape, G. W. Collins, R. Jeanloz, and R. J. Hemley, "Insulator-metal transition in dense fluid deuterium," Science **361**, 677–682 (2018).

[28]D. K. Bradley, J. H. Eggert, D. G. Hicks, P. M. Celliers, S. J. Moon, R. C. Cauble, and G. W. Collins, "Shock compressing diamond to a conducting fluid," Phys. Rev. Lett. **93**, 195506 (2004).

[29]M. Guarguaglini, J. A. Hernandez, T. Okuchi, P. Barroso, A. Benuzzi-Mounaix, M. Bethkenhagen, R. Bolis, E. Brambrink, M. French, Y. Fujimoto, R. Kodama, M. Koenig, F. Lefevre, K. Miyanishi, N. Ozaki, R. Redmer, T. Sano, Y. Umeda, T. Vinci, and A. Ravasio, "Laser-driven shock compression of "synthetic planetary mixtures" of water, ethanol, and ammonia," Sci. Rep. **9**, 10155 (2019).

©Author(s) 2020